

PAPER • OPEN ACCESS

Processing effects on tensile superelastic behaviour of $\text{Fe}_{43.5}\text{Mn}_{34}\text{Al}_{15 \pm x}\text{Ni}_{7.5 \mp x}$ shape memory alloys

To cite this article: M Popa *et al* 2019 *IOP Conf. Ser.: Mater. Sci. Eng.* **591** 012026

View the [article online](#) for updates and enhancements.

Processing effects on tensile superelastic behaviour of $\text{Fe}_{43.5}\text{Mn}_{34}\text{Al}_{15\pm x}\text{Ni}_{7.5\mp x}$ shape memory alloys

M Popa¹, B Pricop¹, R-I Comaneci¹, G Gurau², M Vollmer³, P Krooss³,
T Niendorf³ and L-G Bujoreanu¹

¹“Gheorghe Asachi” Technical University of Iasi, Faculty of Materials Science and Engineering, Blvd. Dimitrie Mangeron 71 A, 700050 Iasi, Romania

²“Dunarea de Jos” University of Galati, Faculty of Engineering, Domneasca Street, 47, 800008 Galati, Romania

³Kassel University, Monckebergstrasse 3, Institute of Materials Technology, D-34125 Kassel, Germany

E-mail: lgbujor@tuiasi.ro

Abstract. $\text{Fe}_{43.5}\text{Mn}_{34}\text{Al}_{15}\text{Ni}_{7.5}$ was introduced in the current decade as a new superelastic alloy with great applicative potential due to: (i) superelastic behaviour over a thermal range of 200°C and (ii) recoverable strains up to 9.7 %. One of the key factors in enhancing the superelastic response of several shape memory alloys (SMAs) is the formation of an oligocrystalline structure, *i.e.* without triple junctions between grains, which is the result of an abnormal grain growth (AGG) process that can be induced by cyclic heat treatment (CHT). Considering that, up to present date, no systematic observations were reported on the effects of Al substitution with Ni, the present study aims to analyse precisely these effects of on the structure and properties of $\text{Fe}_{43.5}\text{Mn}_{34}\text{Al}_{15-x}\text{Ni}_{7.5+x}$, where $x = 0$; 1.5 and 3 at. %. The ingots with the five above mentioned compositions were: (i) cut by wire electrical discharge machining (WEDM); (ii) hot rolled (HR) at 1060°C with 43.7-70 % thickness reduction degrees; (iii) annealed (A) at 900°C/ 1h/ water, (iv) cold rolled (CR) with 60-92.7 % thickness reduction degrees; (v) cut by WEDM under the configuration of tensile specimens; (vi) subjected to CHT between 1225 and 900°C with heating-cooling rates of 10°C/ min (repeated three times) and final water cooling to 80°C before being subjected to (vii) final ageing (AT) at 200°C for 3 hours/ water. After applying this complex thermomechanical procedure, the specimens were analysed by optical microscopy (OM) and the average diameter of crystalline grains was calculated based on dimensional measurements. Considering that the approximate specimen thickness was 1 mm, since the average grain size of thermomechanically treated specimens ranged between 1.3 and 3.7 mm, it can be concluded that oligocrystalline structure, characterized by grain size larger than specimen's thickness/ diameter has been obtained. Tensile tests were performed on thermomechanically treated specimens, both up to failure and by loading-unloading. The evolution of average hardness, during the five processing stages, HR-A-CR-CHT and AT was determined and discussed.

1. Introduction

Superelastic behaviour is currently associated with a stress plateau or at least an inflection point on the unloading path of a loading-unloading curve [1] enabling to obtain recoverable strains up to 25 % [2]. The mechanism of superelastic behaviour is based on a reversible thermoelastic martensitic



transformation (stress-induced martensite plates continuously grow during isothermal loading and continuously shrink back during isothermal unloading), which requires the presence of highly reinforced parent phase (austenite), by high crystallographic ordering or by coherent precipitation [3].

At the beginning of the present decade the discovery of oligocrystalline $\text{Fe}_{43.5}\text{Mn}_{34}\text{Al}_{15}\text{Ni}_{7.5}$ alloy, experiencing stable superelastic behaviour between -50 and $+150^\circ\text{C}$, opened the path for the development of large scale seismic applications in civil engineering, being promoted by their increased cost efficiency [4]. In order to enable the reversibility of stress induced γ' -face centred cubic (fcc) martensite, the α -body centred cubic (bcc) austenite has to be strengthened by coherent precipitation of ordered β -NiAl-bcc [5]. Additionally, to matrix-reinforcement by coherent precipitates, superelastic behaviour is enhanced by the absence of triple junctions between grains, which is the main feature of oligocrystalline structures [6], characterized by super unity value of the ration between average grain size and specimen thickness or width [7]. Such “bamboo type” structures are formed after a cyclic heat treatment, around solvus temperature, by a discontinuous phenomenon called abnormal grain growth [8], that occurs in particular grains that grow faster by consuming the surrounding smaller ones [9].

Taking into account large scale applications, the research group coordinated by Professor Kainuma, issued one patent on the production method of $\text{FeMnAlNi}(\text{SiTiVCrCoCuMoWBC})$ alloys, represented by $\text{Fe}_{43.5}\text{Mn}_{34}\text{Al}_{15}\text{Ni}_{7.5}$, “with relatively low cost, excellent workability and high shape memory effect and hyperelasticity” [10]. They further improved their findings by reporting a patent on corrosion-resistant $\text{Fe}_{18-55.9}\text{Mn}_{25-42}\text{Al}_{9-13}\text{Ni}_{5-12}\text{Cr}_{5.1-15}$ [11].

In their studies Kainuma *et al* did not investigated the effects of substituting Al, an alpha forming element with Ni, gamma forming one. This why the present paper aims to characterize the microscopic and macroscopic changes, induced by slight substitutions (± 1.5 at. % and (± 3 at. %) of Al with Ni around “classic” composition $\text{Fe}_{43.5}\text{Mn}_{34}\text{Al}_{15}\text{Ni}_{7.5}$.

2. Experimental procedure

Five groups of cylindrical ingots, with nominal chemical composition $\text{Fe}_{43.5}\text{Mn}_{34}\text{Al}_{15\pm X}\text{Ni}_{7.5\mp X}$ ($X = 0; 1.5$ and 3 % at.%) were melt in cold crucible induction furnace, cast into copper moulds and roughly machined before being longitudinally cut by wire electric discharge machine (WEDM). The parallelepipedic fragments were thermomechanically processed, passing through the five consecutive states: (i) HR-hot rolling (1060°C , $43.75 - 70\%$ thickness-reduction); (ii) A-annealing ($900^\circ\text{C}/1\text{h}$ / water quenching, WQ); (iii) CR-cold rolling ($60 - 92.7\%$ thickness-reduction); (iv) CHT-cyclic heat treatment ($1225^\circ\text{C}/0.5\text{h}$), repeated three times with a heating-cooling rate of $10^\circ\text{C}/\text{min}$, followed by solution treatment ($1225^\circ\text{C}/1\text{h}$ / WQ at 80°C) in quartz evacuated capsules, partially filled with Ar) and (v) AT-ageing ($200^\circ\text{C}/3\text{h}$ / WQ). The thermomechanical procedure is shown in figure 1.

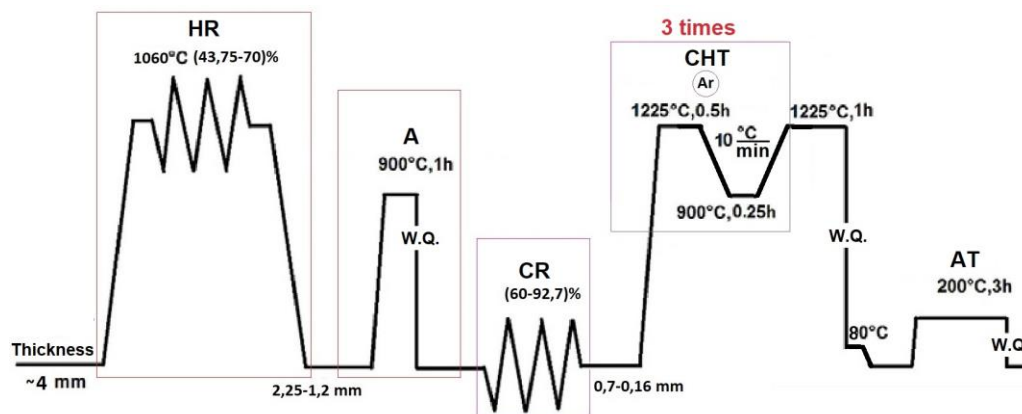


Figure 1. Schematic thermomechanical processing comprising: HR-hot rolling, A-annealing, CR-cold rolling, CHT-cyclic heat treatment and AT-ageing.

Samples of each of the above processing states, from each of the five alloy systems, were metallographically prepared for optical microscopy (OM) by grinding and automatic polishing on a METKON FORCIPOL 1V machine, before being etched with 8.5 CuSO₄, 8.5 H₂O, 33 CH₃-CH₂-OH and 50 HCl (%vol) solution after heating to about 50°C with a hot-air gun, in order to selectively corrode the metallographic constituents.

By WEDM, dog bone specimens with gauge dimensions of 3×2×0.7 mm³ were cut. Tensile tests, with a strain of 2 % per cycle, were conducted on an INSTRON 3382 testing machine. Micro-hardness measurements under a load of 100 g were repeated seven times for each specimen condition. Medium micro-hardness (mHV_{100,med}) was determined as an average of five remaining values, after the elimination of two isolated results.

3. Experimental results and discussion

The OM micrographs of the samples after the first three processing steps are illustrated in figure 2.

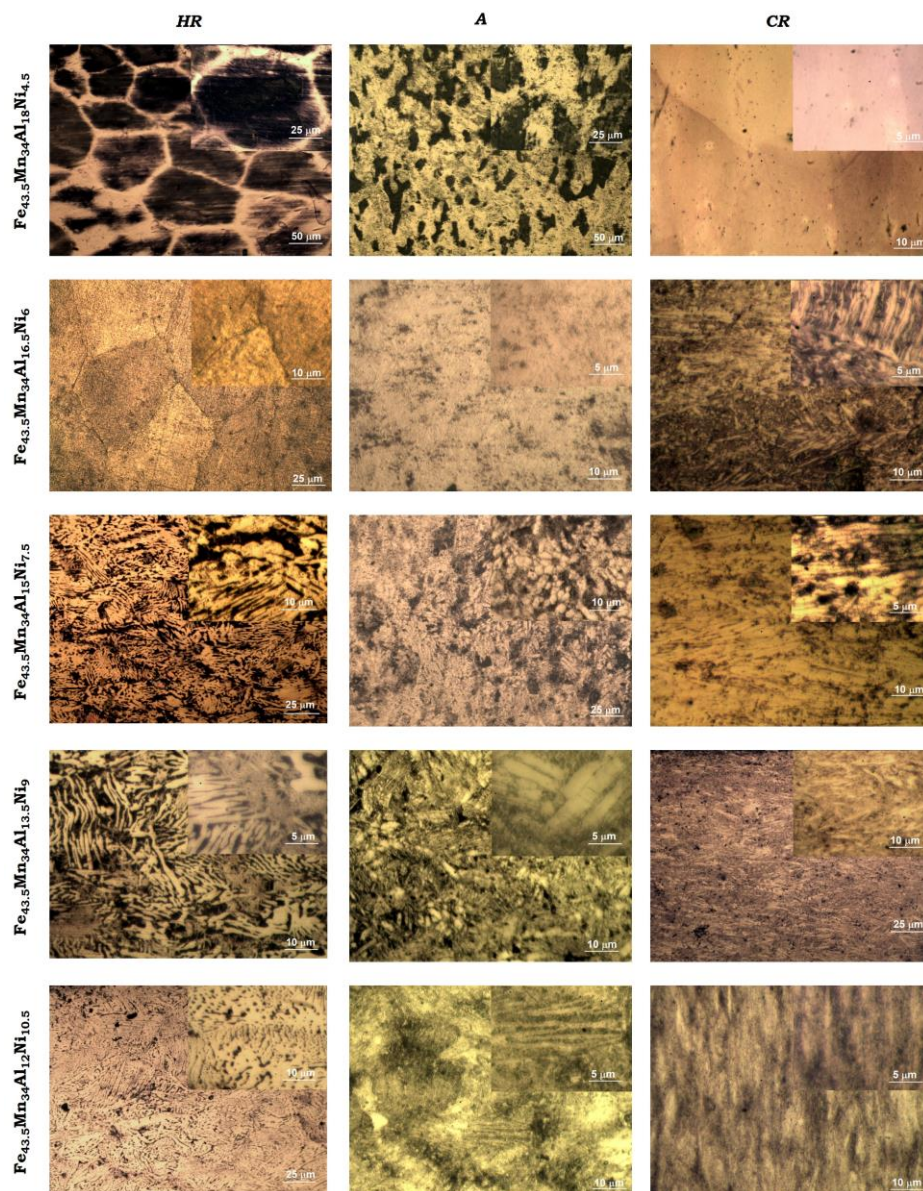


Figure 2. OM micrographs after the first three processing steps.

It is obvious from figure 2 that all the conditions exhibit an $\alpha + \gamma$ two phase microstructure. In the first three processing steps, as compared to “classical” $\text{Fe}_{43.5}\text{Mn}_{34}\text{Al}_{15}\text{Ni}_{7.5}$ alloy, it appears that Ni-lean alloys have large α -bcc grains with allotriomorph γ -fcc islets while Ni-rich alloys display much finer elongated γ -fcc grains that caused fibering structure after cold rolling. $\text{Fe}_{43.5}\text{Mn}_{34}\text{Al}_{15}\text{Ni}_{7.5}$ specimens, in hot rolled state, comprises α -bcc grains with an average size of about 0.5 mm with acicular γ -fcc precipitated along grain boundaries.

After the fourth processing step, abnormal grain growth occurred as illustrated in figure 3.

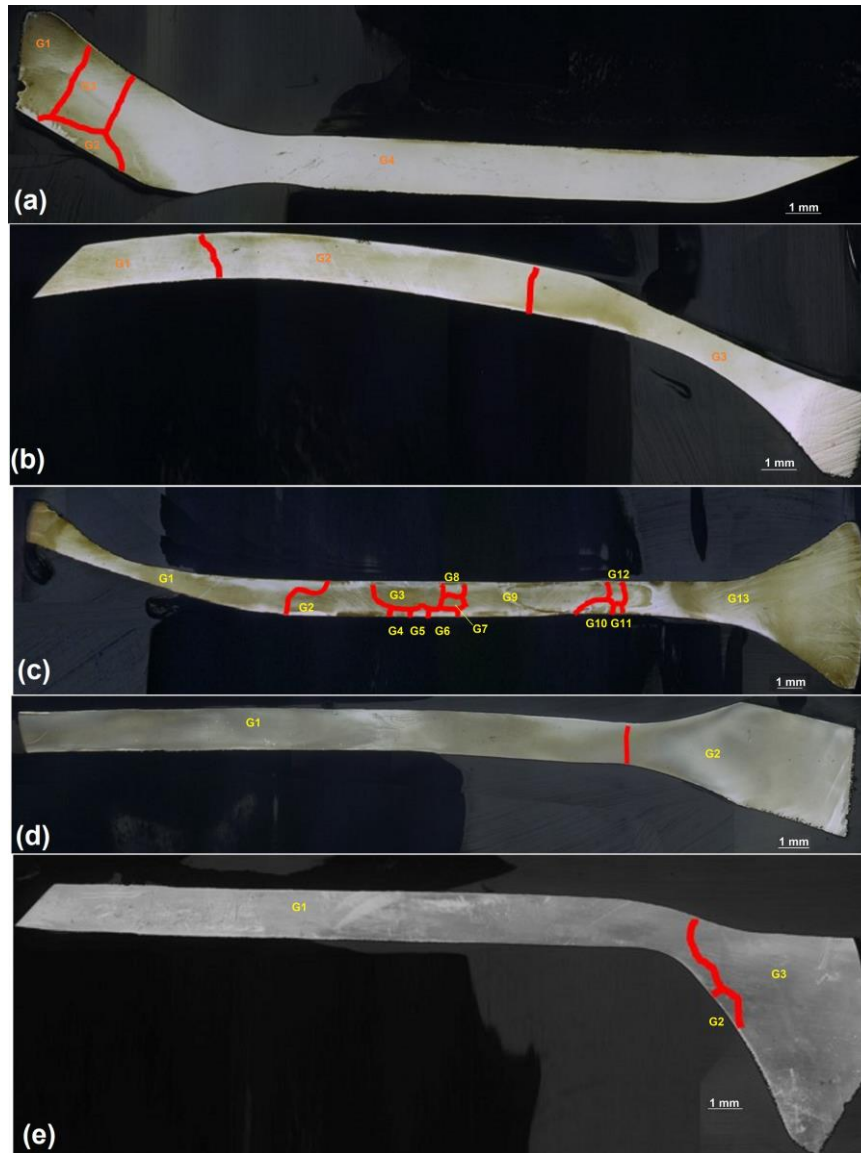


Figure 3. Grain boundaries observed, after CHT, at tensile specimens with different chemical composition: (a) $\text{Fe}_{43.5}\text{Mn}_{34}\text{Al}_{18}\text{Ni}_{4.5}$; (b) $\text{Fe}_{43.5}\text{Mn}_{34}\text{Al}_{16.5}\text{Ni}_6$; (c) $\text{Fe}_{43.5}\text{Mn}_{34}\text{Al}_{15}\text{Ni}_{7.5}$; (d) $\text{Fe}_{43.5}\text{Mn}_{34}\text{Al}_{13.5}\text{Ni}_9$; (e) $\text{Fe}_{43.5}\text{Mn}_{34}\text{Al}_{12}\text{Ni}_{10.5}$.

In figure 3, grain boundaries were marked with red colour and numbered as G_i . Figure 3(a) shows that abnormal grain growth occurred after CHT, in specimen $\text{Fe}_{43.5}\text{Mn}_{34}\text{Al}_{18}\text{Ni}_{4.5}$, so that the right-side grain, G_4 , reached 19.5 mm maximum dimension, while specimen's width is 1.5 mm. The presence of triple junctions between grains does not recommend the chemical composition $\text{Fe}_{43.5}\text{Mn}_{34}\text{Al}_{18}\text{Ni}_{4.5}$ for further tensile test. Figure 3(b) shows that the specimen $\text{Fe}_{43.5}\text{Mn}_{34}\text{Al}_{16.5}\text{Ni}_6$ developed oligocrystalline

structure after CHT, since only three grains are noticeable along specimen's surface. Average maximum dimensions of the grains G_2 and G_3 have been about 9 mm. Surprisingly, at the "classic" $\text{Fe}_{43.5}\text{Mn}_{34}\text{Al}_{15}\text{Ni}_{7.5}$ specimens, CHT generated thirteen grains with varying dimensions between 0.2 and 12 mm, as illustrated by figure 3(c). The most oligocrystalline specimen, after CHT, has been undoubtedly $\text{Fe}_{43.5}\text{Mn}_{34}\text{Al}_{13.5}\text{Ni}_9$ that developed only 2 grains, according to figure 3(d). In this case, the largest grains exceed 19 mm in length. Finally, at $\text{Fe}_{43.5}\text{Mn}_{34}\text{Al}_{12}\text{Ni}_{10.5}$ CHT developed three grains, among which G_2 was not completely "consumed" by its G_3 neighbour.

For accurate grain size measurements, the surface (S) and perimeter (P) of each G_i grain were measured and the equivalent diameter (D_{equiv}) of the circular equivalent grain was determined with equation (1):

$$D_{\text{equiv}} = 4S/P \quad (1)$$

The average grain size, D_{ave} , was finally determined as an arithmetic average of equivalent diameters. The results are summarized in table 1.

Table 1. Calculation of equivalent and average diameters of crystalline grains, induced by CHT, according to figure 3.

Specimen		$\text{Fe}_{43.5}\text{Mn}_{34}\text{Al}_{18}\text{Ni}_{4.5}$	$\text{Fe}_{43.5}\text{Mn}_{34}\text{Al}_{16.5}\text{Ni}_6$	$\text{Fe}_{43.5}\text{Mn}_{34}\text{Al}_{15}\text{Ni}_{7.5}$	$\text{Fe}_{43.5}\text{Mn}_{34}\text{Al}_{13.5}\text{Ni}_9$	$\text{Fe}_{43.5}\text{Mn}_{34}\text{Al}_{12}\text{Ni}_{10.5}$
G_1	S	mm ²	3.21	5.92	20.27	25.56
	P	mm	8	11.4	28.8	41.1
	D_{equiv}	mm	1.605	2.072	2.817	2.489
G_2	S	mm ²	0.97	12.55	4.93	20.45
	P	mm	5.7	20.4	11.1	16.3
	D_{equiv}	mm	0.68	2.457	1.775	5.034
G_3	S	mm ²	2.81	16.63	3.11	-
	P	mm	6.8	22.9	8.3	-
	D_{equiv}	mm	1.655	2.91	1.493	-
G_4	S	mm ²	28.57	-	0.33	-
	P	mm	26.4	-	2.7	-
	D_{equiv}	mm	4.324	-	0.494	-
G_5	S	mm ²	-	-	0.26	-
	P	mm	-	-	2.2	-
	D_{equiv}	mm	-	-	0.468	-
G_6	S	mm ²	-	-	0.44	-
	P	mm	-	-	3.3	-
	D_{equiv}	mm	-	-	0.529	-
G_7	S	mm ²	-	-	0.63	-
	P	mm	-	-	3.3	-
	D_{equiv}	mm	-	-	0.757	-
G_8	S	mm ²	-	-	0.63	-
	P	mm	-	-	3.2	-
	D_{equiv}	mm	-	-	0.783	-
G_9	S	mm ²	-	-	8.64	-
	P	mm	-	-	15	-
	D_{equiv}	mm	-	-	2.304	-
G_{10}	S	mm ²	-	-	0.78	-
	P	mm	-	-	3.9	-
	D_{equiv}	mm	-	-	0.802	-
G_{11}	S	mm ²	-	-	0.25	-
	P	mm	-	-	2	-
	D_{equiv}	mm	-	-	0.5	-
G_{12}	S	mm ²	-	-	0.59	-
	P	mm	-	-	3.1	-
	D_{equiv}	mm	-	-	0.759	-
G_{13}	S	mm ²	-	-	30.32	-
	P	mm	-	-	27.1	-
	D_{equiv}	mm	-	-	4.474	-
D_{ave}	mm	2.066	2.48	1.381	3.761	2.175

It is noticeable that the only specimens with oligocrystalline structure, $\text{Fe}_{43.5}\text{Mn}_{34}\text{Al}_{16.5}\text{Ni}_6$ and $\text{Fe}_{43.5}\text{Mn}_{34}\text{Al}_{13.5}\text{Ni}_9$ have the largest average grain size, namely 2.48 and 3.761 μm , respectively. In addition, the specimen with “classic” chemical composition, $\text{Fe}_{43.5}\text{Mn}_{34}\text{Al}_{15}\text{Ni}_{7.5}$, which did not develop oligocrystalline structure after CHT, had the least average grain size, 1.381 μm and for this reason it was excluded from further tensile experiments. Figure 4 summarizes stress-strain variations, during mechanical cycling, of the specimens the gauges of which developed oligocrystalline structure after cyclic heat treatment. Even if some specimens revealed triple junctions, they were located in the grip-fastening area so they would not influence tensile superelastic behaviour.

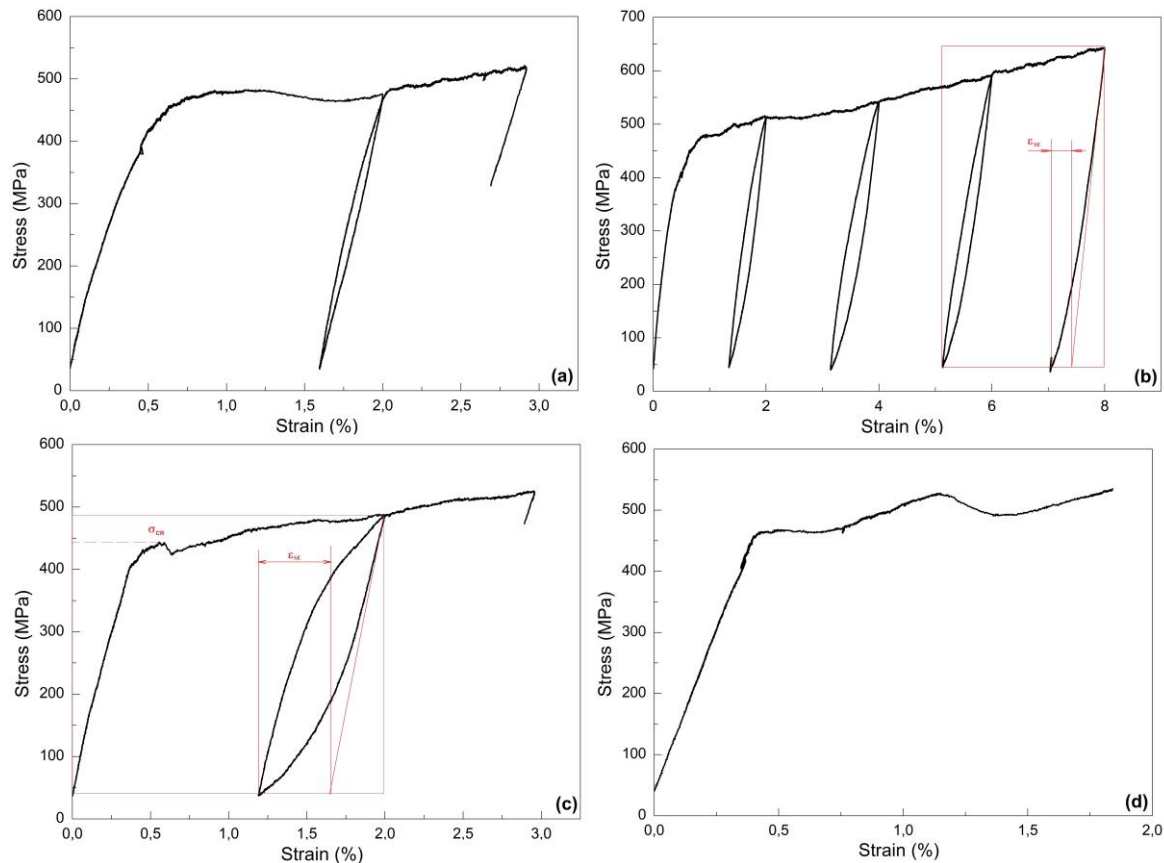


Figure 4. Mechanical cycling results of the specimens that developed oligocrystalline structures, along their gauges, after cyclic heat treatment: (a) $\text{Fe}_{43.5}\text{Mn}_{34}\text{Al}_{18}\text{Ni}_{4.5}$; (b) $\text{Fe}_{43.5}\text{Mn}_{34}\text{Al}_{16.5}\text{Ni}_6$; (c) $\text{Fe}_{43.5}\text{Mn}_{34}\text{Al}_{13.5}\text{Ni}_9$; (d) $\text{Fe}_{43.5}\text{Mn}_{34}\text{Al}_{12}\text{Ni}_{10.5}$.

The specimens $\text{Fe}_{43.5}\text{Mn}_{34}\text{Al}_{16.5}\text{Ni}_6$ and $\text{Fe}_{43.5}\text{Mn}_{34}\text{Al}_{13.5}\text{Ni}_9$, with oligocrystalline structure and largest grain size, experience the most obvious superelastic response. Thus, specimen $\text{Fe}_{43.5}\text{Mn}_{34}\text{Al}_{16.5}\text{Ni}_6$ that had only three grains, in figure 3(b), resisted four loading-unloading cycles, during which maximum stress increased with approx. 100 MPa. In the last cycle, total strain reached 2.9 % (per cycle), total recovery strain was 0.9 % and the superelastic strain, ϵ_{SE} , was 0.4 %, according to figure 4(b). In figure 4(c) the specimen $\text{Fe}_{43.5}\text{Mn}_{34}\text{Al}_{13.5}\text{Ni}_9$, which revealed only two grains in figure 3(d), reached the stress plateau at approx. 443 MPa and developed a superelastic strain $\epsilon_{\text{SE}} \approx 0.47$ %.

The results of microhardness (mHV) measurements are summarized in figure 5 for the first three processing states, hot rolled, annealed and cold rolled.

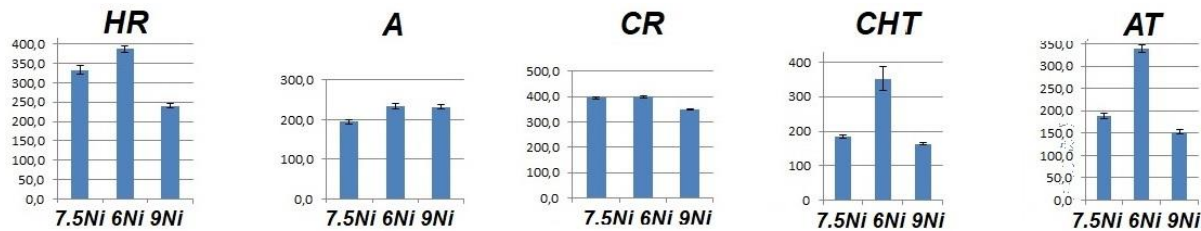


Figure 5. mHV values illustrating the effects of ± 1.5 at% Al substitution with Ni, during the 5 processing steps.

It is noticeable that the specimen with classic chemical composition, $\text{Fe}_{43.5}\text{Mn}_{34}\text{Al}_{15}\text{Ni}_{7.5}$, had the largest mHV values in most of the five processing steps. In addition, it is the only one that experienced softening, after annealing and hardening after cyclic heat treatment and ageing.

4. Conclusions

By summarizing the above results the following conclusions can be drawn:

- annealing induced softening, cold rolling caused fibering, in Ni-rich specimens, but did cause obvious microhardness (mHV) increases.
- by cyclic heat treatment, oligocrystalline structures were obtained, in specimens $\text{Fe}_{43.5}\text{Mn}_{34}\text{Al}_{13.5}\text{Ni}_9$ and $\text{Fe}_{43.5}\text{Mn}_{34}\text{Al}_{16.5}\text{Ni}_6$ which developed the largest average grain sizes (D_{ave}) 3.761 and 2.48 mm, respectively, while the rest of the specimens had $D_{\text{ave}} > 2$ mm, expecting for specimen $\text{Fe}_{43.5}\text{Mn}_{34}\text{Al}_{15}\text{Ni}_{7.5}$ that revealed fibering, after cold rolling.
- in oligocrystalline specimens $\text{Fe}_{43.5}\text{Mn}_{34}\text{Al}_{13.5}\text{Ni}_9$ and $\text{Fe}_{43.5}\text{Mn}_{34}\text{Al}_{16.5}\text{Ni}_6$ superelastic strains of 0.47 % and 0.4 % were observed, respectively.

5. References

- [1] Duerig T W and Zadno R 1990 An engineer's perspective of pseudoelasticity *Engineering Aspects of Shape Memory Alloys* Eds. Duerig T W, Melton K N, Stockel D, Wayman C M, (Oxford: Butterworth-Heinemann) p 369
- [2] Oliveira J P, Zeng Z, Berveiller S, Bouscaud D, Braz Fernandes F M, Miranda R M and Zhou N 2018 *Mater Design* **148** 145
- [3] Wayman C M 1975 Deformations, mechanisms and other characteristics of shape memory alloys *Shape Memory Effects in Alloys* Ed. Perkins J (New York: Plenum Press) p 1
- [4] Omori T, Ando K, Okano M, Xu X, Tanaka Y, Ohnuma I, Kainuma R and Ishida K 2011 *Science* **333** 68
- [5] Tseng L W, Ma J, Hornbuckle B C, Karaman I, Thompson G B, Luo, Z P and Chumlyakov Y I 2015 *Acta Mater* **97** 234
- [6] Ueland S M, Chen Y and Schuh C A 2012. *Adv Funct Mater* **22** 2094
- [7] Omori T, Okano M and Kainuma R 2013 *Appl Phys A Mater* **1** 032103
- [8] Omori T, Iwaizako H and Kainuma R 2016 *Mater Design* **101** 263
- [9] Omori T, Kusama T, Kawata S, Ohnuma I, Sutou Y, Araki Y, Ishida K and Kainuma R 2013 *Science* **341** 1500
- [10] Ishida K, Kainuma R, Ohnuma I, Omori T and Ando K 2014 Patent No.: *US 8,815,027 B2*
- [11] Omori T, Kainuma R, Noguchi Y, Kise S and Tanaka T 2019 Patent No.: *US 2019/ 0153571 A1*

Acknowledgments

This work was supported by UEFISCDI through project code PN-III-P4-ID-PCE-2016-0468, contract no. 76/2017.